UNIVERSITY OF BIRMINGHAM

University of Birmingham Research at Birmingham

Using broadband seismic networks to optimise microgravity survey strategy in the UK

Goncharenko, Yuriy; Boddice, Daniel; Rodgers, Anthony; Atkins, Philip; Metje, Nicole; Chapman, David

[Link to publication on Research at Birmingham portal](#)

Using broadband seismic networks to optimise microgravity survey strategy in the UK

Yuriy Goncharenko[1], Daniel Boddice[2*], Anthony Rodgers[2], Philip Atkins[2], Nicole Metje[2], David Chapman[2]

1. Microwave Systems Laboratory, Dept. of Electrical and Computer Engineering, Colorado State University, Fort Collins, CO 80523 USA (formerly of 2)

2. School of Engineering, College of Engineering and Physical Sciences, University of Birmingham, Edgbaston, Birmingham, B15 2TT

* Corresponding author; email:d.boddice@bham.ac.uk

Abstract

Microgravity measurements are a useful tool for detecting subsurface features, especially deep targets or those in conductive ground which lie outside the capabilities of other methods based on electromagnetic signal transmission. However, the method is limited by a range of noise sources including vibrational noise from the environment, one source of which comes from microseism noise due to ocean waves. This noise travels through the bedrock and manifests itself in the data. It varies as a function of time and location. The effect of the wave noise on microgravity measurements in the UK was assessed for the first time using a field gravimeter (Scintrex CG5) and a link was demonstrated between the noise from microgravity measurements and those from a broadband seismometer. As a result, a new method for assessing the impact of this noise on microgravity measurements in the UK is proposed using readily available data from the continuously monitoring seismic network run by the British Geological Survey (BGS) to create an accurate nowcast. Knowledge of this noise on the day of survey in conjunction with an approximate signal strength of the expected targets can be used to significantly improve survey planning in terms of the optimal observation time at which surveys for particular targets should be conducted, saving time and money on failed microgravity surveys.

Keywords: Gravity, Signal processing, Seismics, Noise, Parameter estimation.

Introduction

Microgravity surveying is an efficient tool for geophysical remote sensing of buried objects. Unlike other active geophysical techniques such as ground penetrating radar (GPR) (Jol, 2009), earth resistance surveying (Keller and Frischknecht, 1966) or electromagnetic induction (Kaufman, Alekseev and Oristaglio, 2014), which rely on the injection of a signal into attenuating ground, the effective depth of penetration of a gravimeter does not depend on the electromagnetic properties of the soil or buried objects, but depends only on the size of the target and the density contrast between the object and surrounding soil. This allows microgravity to be used to find deep targets, those buried in electrically conductive ground such as clay-rich or water-saturated soils or those screened by reinforced concrete, where none of the techniques mentioned above are effective (Jol, 2009; Kaufman et al., 2014; Keller and Frischknecht, 1966). Nevertheless, there is a significant limiting factor for the wide usage of existing gravimeters: the signal-to-noise ratio (expressed as a ratio between the signal power and the noise power) for such measurements does not exceed a factor of 3-5 and very often falls below 1. Whilst many studies have concentrated on the understanding and correction of low frequency sources of noise, which affect the accuracy of a survey between readings over the whole survey day such as tides (e.g. Hartmann and Wenzel, 1995) and atmospheric pressure (e.g. Merriam, 1992; Warburton and Goodkind, 1977), much less attention has been given to noise sources which affect the accuracy of individual microgravity estimates over a single measurement cycle. There are three main sources of the microgravity noise for single-point measurements:

- internal noise of the sensor (e.g. mechanical relaxation of the spring in Micro-Electro Mechanical System (MEMS) gravimeters and electronics flicker noise)

- external environmental noise (e.g. ambient microgravity microseism noise (Ardhuin et al., 2011; Hasselmann, 1963; Traer et al., 2012) and vibrations caused by wind)

- external man-made noise (e.g. vibrations from road traffic, construction work and pedestrians (Wilson, 1953))

Internal noise has a broadband nature and is defined by the sensor. The instrument noise consists of white noise caused by thermal noise of electronic components and 1/frequency (flicker) noise caused by recombination effects occurring at defects in the semiconductor volume. The only way to decrease it is by using low-temperature stabilised electronics or to move from mechanical mass and spring gravimeters to superconducting (Goodkind, 1999) or atom interferometry sensors (Metje et al., 2011; Peters, Chung and Chu, 1999; Snadden et al., 1998), but current designs are not yet developed for field survey conditions. Nevertheless, significant developments of cold atom gravimeters have occurred in recent years (Bidel et al., 2013; Gillot et al., 2016; Hinton et al., 2017), with commercially available mobile laboratory instruments now available (Muquans, 2017) and it is likely that a field capable instrument will follow by 2019 as part of the REVEAL[1] project.

Vibrations from man-made sources and the wind usually have an impulsive and high-frequency nature and can be rejected using non-linear filtering or despiking techniques (Hassanpour, Mesbah and Boashash, 2004). In terms of environmental noise, microseism noise possesses a peak frequency much lower in the spectral content than wind and anthropogenic vibration noise sources, and is therefore difficult to filter

---

[1] http://gow.epsrc.ac.uk/NGBOViewGrant.aspx?GrantRef=EP/R000220/1

without affecting the signal-of-interest. The only way of removing this noise is by integrating the signal over a long time period.

Figure 1 shows the noise spectra from two Scintrex CG5 instruments which were run simultaneously for 36 hours at the same location. At higher frequencies the instruments show similar noise responses, showing that the environmental noise is dominant. However, at periods longer than the maximum measurement time of the instrument (256 seconds), it can be seen that the noise sources are dissimilar between the two instruments and therefore the instrument specific noise sources are dominant. Since these noise sources are impossible to eliminate but are also independent of environmental conditions, this paper will focus on the assessment of the higher frequency microseism noise.

Microseism noise is caused by pressure changes on the ocean floor due to the action of waves in the open ocean (Ardhuin et al., 2011; Hasselmann, 1963). The resulting noise on gravity measurements are the sum of different wave groups which are propagated by three different pathways (Traer et al., 2012):

1. Primary microseisms ($0.04 - 0.17$ Hz), first described by Hasselmann (1963), are formed due to the interaction between waves and the fixed ocean floor which creates vertical oscillations and resulting seismic waves. According to Ardhuin et al., (2015) the peak period is approximately 15 seconds.

2. Double-frequency (DF) microseisms ($0.08 - 0.34$ Hz) are formed at twice the frequency of primary microseisms due to the interaction between different wave groups or reflected and incident waves (Ardhuin et al., 2011). According to Ardhuin et al. (2015), the peak period is approximately 5 seconds.

3. Seismic hum (> 0.03 Hz) which is caused by swell-transformed infragravity wave interactions. According to Webb (2008), the power is 300 times smaller than that of DF microseisms. These frequencies are too low to be observed within gravity measurements and are masked by much stronger instrument noise at these frequencies.

The resulting microseism noise that can be observed in gravity measurements is dependent on seasonal and weather conditions in the open ocean (Ardhuin et al., 2015; Ardhuin and Herbers, 2013; Ardhuin et al., 2011) and is located in the range of 0.1-0.3 Hz with a bandwidth of approximately 0.05-0.5 Hz. The typical variation of the standard deviation of the microseism noise, obtained on 11th -27th February 2016 using a Scintrex CG5 gravimeter in the basement of a building in the University of Birmingham, UK, is shown in Figure 2. The highest standard deviation of the microseism noise was observed on 20th February 2016 (line A on Figure 2) and the quietest time was on 25th February 2016 (line B on Figure 2). The variations of the significant wave height (defined as the average height of the highest one-third of the waves, which in deep water equates to four times the square root of the zeroth moment of the narrow band energy spectrum (Phillips, 1977; Sverdrup and Munk, 1947), observed at the same time in Cornwall (station Wave Hub; GeoData Institute, 2015) are also shown in Figure 2. It is clearly visible that the standard deviation of the microseism noise is strongly dependent on the significant wave height.

Waveforms and spectra of the microseism noise are shown in Figures 3 and 4. The signal is formed of the convolution of primary and secondary microseisms (Essen et al., 2003; Yang and Ritzwoller, 2008), which makes the resulting signal only partially deterministic over the measurement cycle due to the imperfect sinusoidal signal

generated. Taking into account that the longest period of the microseism noise (20 s, according to Figure 4) is comparable with the duration of an individual microgravity measurement (typically 30 - 60 s), the influence of this type of environmental noise becomes very significant and potentially detrimental to identifying the signal-of-interest. One solution to this is to increase the measurement time in order to reduce the uncertainty by averaging multiple cycles of the unwanted signal, but this is time consuming and greatly adds to the time needed for data acquisition. This results in significant cost implications making it undesirable, especially in the commercial sector. The efficiency of long-term averaging of data depends also on the level of flicker noise, which becomes more significant at lower frequencies (i.e. longer averaging intervals). For each specific instrument, the optimal duration of averaging is different, but for a Scintrex CG-5 does not exceed a few minutes.

The estimation of the microgravity signal follows a signal flow chain as shown in Figure 5. The gravity signal corresponding to the desired target, $s(t)$, is assumed to be constant. Thus the corresponding spectrum, $S(f)$, is assumed to be a delta function occurring at zero frequency, $\delta(0)$. This signal is contaminated with zero mean additive noise and power spectral density, $G(f)$. The measured signal is passed through a linear time invariant filter with transfer function $H(f)$. Thus the estimated noise power is

$$\sigma^2 = \int_{-\infty}^{+\infty} |H(f)|^2 G(f) \ df \tag{1}$$

Whilst the signal power occurring at a time t_0 is proportional to

$$A^2 = \left| \int_{-\infty}^{+\infty} H(f)S(f)\exp^{j\omega t_0} \ df \right|^2 \tag{2}$$

The objective is to choose an appropriate linear time invariant filter, $H(f)$, such that the signal-to-noise ratio A^2/σ^2 is maximised. In the absence of knowledge of the noise spectrum, $G(f)$, a rectangular smoothing function is frequently chosen for the filter.

$$h(t) = \frac{1}{\tau} \quad \text{for} \quad -\frac{\tau}{2} < t < \frac{\tau}{2}$$
$$h(t) = 0 \quad \text{elsewhere}$$

(3)

Corresponding to

$$H(f) = \frac{\sin(\pi f \tau)}{\pi f \tau}$$

(4)

This is optimal for white noise, corresponding to the region shown in Figure 1 annotated with a slope of 0 dB per decade. Analytic solutions may be derived for optimal choices of $H(f)$ for regions with transfer functions proportional to f^{const} (e.g. slopes of -20 dB per decade). For more complicated cases such as the microseism spectral content illustrated in Figure 1, the characteristics of $H(f)$ must be derived following a measurement of the noise spectrum, $G(f)$.

Figure 6 shows the typical differences between the assumption that the noise variance reduces linearly with observation time and a rigorously evaluated performance metric showing a much reduced performance. Typically, the noise reduction is a factor of five worse for nominal observation times of between 10 seconds and 100 seconds. Observation times should always be greater than the period of the microseisms and long observation times in excess of 100 seconds are relatively ineffective.

As mentioned above, the peak frequency and power of microseism noise depends on weather conditions in the nearshore zone and in the open ocean. The power of

microseism noise also depends on the distance from the measuring point to the source of the noise (e.g. the ocean) and underlying bedrock and sedimentary formation (Field and Jacob, 1993). It is therefore apparent that microseism noise significantly varies both temporally and spatially across the UK and worldwide and that the evaluation of the expected power of microseism noise for a given site and day is invaluable for choosing the most efficient strategy of microgravity survey in terms of measurement time-per-point. To date, no estimation or map exists that can predict this noise source for microgravity and thus support the survey planning.

The simplest way to collect information about spatial and seasonal dependencies of the microseism noise would be to establish a permanent network of closely-spaced broadband microgravity sensors and collect data continuously. However, there are many financial, technical and organizational challenges to establishing such a network of gravity stations for continuous monitoring making this an unrealistic approach and therefore it is more viable to use existing databases. Both ambient seismic noise (Yang and Ritzwoller, 2008), which is well known in seismology and can be measured by broadband seismic stations (British Geological Survey, 2016), and the microseism noise which affects microgravity readings have a common source: the interaction between ocean waves and the ocean floor. This research investigates the relationship between those two processes and uses data obtained from the British Geological Survey (BGS)'s seismic network to build a map of microseism noise for the UK. It establishes whether this approach is suitable to provide a much better understanding of the microseism noise with the enormous potential benefit for survey planning.

The relationship between gravity microseism noise and seismic microseism noise

In order to show the relationship between ambient seismic and ambient microgravity wave noise, 1-hour microgravity readings were taken close to five broadband seismic stations in the UK. Three of them were located in the North-East of England (Yorkshire and Lincolnshire), one in the East Midlands (Leicestershire) and one in Wales. The names and positions of the processed stations are shown by black diamonds in Figure 7. The positions of other monitoring stations belonging to the BGS's seismic network are shown by grey squares.

Data were collected between December 2015 and January 2016 for different weather conditions ranging from calm weather to a strong winter storm (storm Eva (Met Office, 2016)). Data were acquired using a Scintrex CG-5 (Scintrex Ltd., 2006) microgravimeter (SN 40867). In order to decrease the influence of the non-microseism noise vibrations caused by wind, a portable windshield was used (Figure 8) and the instrument was placed away from tall trees to avoid vibrations caused from root movement. This proved effective as in winds with gusts of up 60 km/h this was shown to offer a factor of improvement of 2.5-3, providing similar data quality to data taken in non-windy conditions. All of the chosen broadband seismic stations were located in remote countryside areas so the level of man-made seismic noise was negligible.

Data Processing

The standard instrument output provides a single value for each reading consisting of averaged data from the whole measurement cycle and applies a noise rejecting seismic filter of an unknown type which distorts the output standard deviation (SD) values, obscuring the information on the microseism noise. Due to this, data were collected

with the instrument raw data logging option enabled to give outputs from the instrument analogue-to-digital converters (ADC) for the gravity, temperature and horizontal (X and Y) tilt with a 6 Hz sampling rate from the internal sensors in a continuously cycling mode, allowing shorter period fluctuations within readings to be studied. Data were subsequently converted from ADC samples to their real values and the gravity data corrected by performing operations according to the methods suggested in the Scintrex CG5 manual (Scintrex Ltd., 2006). This is usually applied automatically in the software before the final readings output in order to ensure that fluctuations in gravity readings were the result of environmental noise only. Firstly, the effects of temperature were compensated using data from the internal temperature sensor, the instrument specific temperature offset (obtained from Scintrex) and the temperature correction coefficient stored in the instrument's embedded software. Secondly, the effects of tilt in the X and Y directions were compensated using a tilt correction. A mistake was found in the formula in the Scintrex CG5's manual for converting the ADC values to tilt angles in arcseconds and the correct version was used and confirmed with Scintrex (Equation 5).

$$X_{obs} = \left(\left((ADC_X\ 0.000076295 - 2.5\ )Sensitivity_X \right) - Offset_X \right)$$

$$Y_{obs} = \left(\left((ADC_Y\ 0.000076295 - 2.5\ )Sensitivity_Y \right) - Offset_Y \right) \qquad (5)$$

Where *ADC* is the value from the analogue-to-digital converter recorded in the data file and *Sensitivity* and *Offset* are the tilt sensitivity and tilt offset values stored in the embedded software during calibration respectively. The correct values of tilt were then used with a $\cos(\theta)$ function to remove deviations from vertical gravity. Tidal noise from celestial bodies was removed using the instrument time-string and location using the same set of formulas used by the instrument's internal software based on formulae

presented by Longman (1959). Finally, the effects of linear creep on the sensor spring causing drift in the readings was removed by fitting a linear trend to the dataset using the polyfit function in Matlab$^®$.

Results

Typically during a commercial microgravity survey, measurements are taken using a few short (30 s or 60 s) readings per point, due to limitations of the instrument software and in order to decrease the overall time of a survey (Seigel, 1995). To represent this during the experiment, the standard deviation of noise was calculated using a 60 s moving window. Preliminary analysis showed that the instantaneous power of the microseism noise was 10-30 times higher than the power of the internal sensor noise (see Figure **Error! Reference source not found.**4), making its effects dominant, so for further analysis the total power of the noise was used as a representation of the power of the microseism noise.

To demonstrate that a coherent relationship existed between the signals measured using the gravimeter and the available seismometer data sets, the cross-correlation coefficient was calculated. The processing chain is illustrated in Figure 9. The continuous seismometer data set available from the seismic network has a nominal sampling rate of 50 Hz and requires resampling at the nominal 6 Hz rate of the gravimeter. The microgravity data was sampled for 256 seconds and this block was integrated and cross-correlated with the seismic data to provide precise time synchronisation. A brute-force search method based on varying the resampling rate and maximising the correlation coefficient was instigated to ensure that the sampling rates of the two data sets agreed to better than 0.1%. Finally, linear regression of the two time-synchronised data sets was

implemented to obtain an 'effective gain' parameter linking the sensitivity of the two instruments to microseism noise.

The results of a typical time synchronisation search are shown in Figure 10. For this example, the time synchronisation offset is clearly identified as occurring at sample 7942 of the seismic data set and no false detections occurred. Correct time synchronisation was experienced with 100% of microgravity measurement analysed. Typical peak correlation values were between 0.05 and 0.25, indicating that significant levels (up to a factor of twenty) of uncorrelated energy existed in one, or both, of the measurements.

Having determined the time and sampling rate synchronisation of the two sources, a linear regression was then performed. A typical result for field measurements correlated with the CWF (Charnwood Forest, Leicestershire, UK) seismic station on 27th December 2015 is shown in Figure 11. The linear regression yields an effective gain of 7.65, implying that the gravimeter is more sensitive to microseism noise than the seismic network. Effective gain values varying between 6.01 (LMK - Market Rasen, Lincolnshire, UK) and 8.32 (EDMD - Edmundbyers, Consett, County Durham, UK) were obtained during the measurement campaign. The microgravity instrument is assumed to be most sensitive to vertical acceleration components and is placed on the boundary between earth and atmosphere. It will thus be exposed to multiple wave types. Seismometers may be mounted at depths of tens of metres where the vertical component may be attenuated by interaction effects with the nearby boundary. Similarly, compliant surfaces (e.g. peaty layers) have been observed to attenuate microseism noise. Thus it is no surprise that the measured effective gain is both greater than unity and varies from location-to-location.

The microgravity ambient noise can now be predicted using the processing stages illustrated in Figure 12. The time-series seismometer network velocity data set, $u(t)$, is transformed to a power spectral density, $|U(\omega)|^2$ (corresponding to the energy contained in each 1 Hz band). An acceleration is obtained by multiplying by $|j\omega|^2$ which is then multiplied by the effective gain determined earlier for each location, $|EG|^2$. Finally, a scaling is applied to output predictions in units of microGals. The efficacy of this process is illustrated in Figure 13 where the solid line represents the measured microgravity noise spectral density and the circles represent the prediction based on measurements recorded at the CWF (Charnwood Forest, Leicestershire, UK) seismic network station.

Survey managers would obviously wish for a simplified, if less precise, prediction tool. This is readily achieved by examination of Figure 13. The majority of the spectral energy is contained within a narrow frequency band, standard practice being to define a centre-frequency based on the geometrical mean of any two equal-amplitude points (typically -6 dB, or -10 dB) on the slopes of the response. This process yields a nominal centre-frequency of 0.25 Hz +/-10% for all the data sets presented within this paper. Thus multiplying the standard deviation of the seismic data by the centre frequency of the microseism (1.58 rad) approximates the differentiation process, then by the worst-case effective gain of 8.32 and finally by 100 to convert to microGals, yields the predicted standard deviation of the microgravity measurements. The remainder of the results presented are based on a simple incoherent prediction that the standard deviation of the microgravity measurements measured in units of microGals are likely to be 1315 times the standard deviation of the seismic network data measured in units of μms^{-1}.

Application of new prediction mechanism to UK

The effectiveness of this very simple incoherent prediction mechanism is demonstrated by means of a scatter plot of standard deviation of seismic noise versus standard deviation of microgravity noise as shown in Figure 14. It should be noted that data from North Yorkshire (HPK), Lincolnshire (LMK) and County Durham (EDMD) were taken during storm Eva and have high standard deviations of microgravity seismic noise. A least squares fit of the observed standard deviation of the microgravity signal to the standard deviation of the ambient seismic noise equates to the simplified incoherent prediction model derived earlier. The level of the microseism noise is based on data collected by the UK broadband seismometer network seismic stations (British Geological Survey, 2016), which can be freely downloaded from the Observatories and Research Facilities for European Seismology (ORFEUS) (Observatories and Research Facilities for European Seismology, 2013). To create a map of the microseism noise across the country (Figure 15) data were used from 20 broadband seismic stations with a wide spatial distribution across the UK (British Geological Survey, 2016). The data were interpolated using a cubic spatial interpolation function (Keys, 1981) to create a georeferenced map of the microseism noise across the UK.

Figure 15a shows the predicted map of the microseism noise for summer conditions (i.e. when wave noise is theoretically lower). The lowest level of background noise (less than 20 microGals) is expected in central England and the highest should be recorded on the Isle of Man (165 microGals) and the North of the Scottish Highlands (159 microGals). Both of those areas are in close proximity to the shoreline, so the observed

result confirms the nature of the ambient seismic and microgravity noise in the UK. The microseism noise distribution, presented in Figure 15b, shows a generally similar spatial distribution of noise. However, the level of background noise recorded on 25th December 2015 is 7-8 times higher than in the summer (1352 microGals on the Isle of Man and 1167 microGals in the North of the UK).

In order to validate the linear regression dependence between ambient seismic and microgravity wave noise, additional measurements were taken in Birmingham, UK (52.48^{o}N, 1.89^{o}W) over several days in the summer and winter 2015-2016. Sixty-minute long records were taken in the sub-basement of the Gisbert Kapp building, University of Birmingham, UK, located at roughly 4 m below the ground without wind noise and with a low level of man-made noise. The comparison between the standard deviation of gravimeter derived microseism noise, calculated from 60-minute raw data records and the values interpolated from the microseism noise maps using the cubic spatial interpolation function (Keys, 1981) is presented in Figure 16. The black line corresponds to the simple prediction model, where measured and predicted values are equal and the circles correspond to the measured and predicted level of noise in Birmingham from the recorded data.

It should be noted that Birmingham (point B in Figures 15a-b) is located far away from the ocean coasts, and the level of the microseism noise is generally lower than in coastal regions such as the South West of the UK or in Scotland. In order to confirm the proposed model in another part of the UK, with a different level of microseism noise, two datasets were taken near Durrington Walls (51.19 ^{o}N, 1.78 ^{o}W; point D in Figure 15a-b), which is part of Stonehenge World Heritage site (UNESCO, 2016). The data were taken on 8th - 9th February 2016 during storm Imogen, so the measured level of

noise is very high. The relationship between the measured and predicted level of noise in Durrington is shown in Figure 16 represented by the stars. Based on Figure 16 it can be concluded that the disagreement between the predicted and measured levels of microseism noise is less than 20% for the range of 40 to 400 microGals and is primarily related to the assumption that the centre frequency of the noise spectrum remains constant.

As shown, the evolution time of microseism noise is strongly dependent on changing weather conditions in the open ocean. The method should therefore be considered alongside weather forecasting models. However, analysis of the data set used in Figure 2 shows that the method has a reasonable success rate at predicting site conditions over the few hours after the nowcast is made. For example, with a window of one hour, 94% of the microgravity standard deviations fall within 50 microGals of the initial prediction which would allow the method to be used as an independent verification and for the methodology of a survey to be adjusted. Over a longer period of 12 hours which would allow the survey date to be altered if necessary, 55% of the microgravity standard deviations fall within 50 microGals of the initial prediction.

Implications for Survey Management Decisions

As mentioned above, the combination of the internal sensor instrument noise and the microseism noise limits the overall accuracy of microgravity measurements, because neither the microseism noise nor the sensor noise can be effectively reduced by currently existing single-sensor MEMS-based gravimeters. This is unlikely to be improved without using a different type of gravity sensor with lower instrumental noise (i.e. super conducting or atom interferometry based gravimeters), and a differential

configuration such as a gradiometer to reduce environmental noise through dynamic cancelling. However, neither of these methods is possible with existing instruments. Thus, the success of any microgravity survey depends strongly on the ratio between the expected signal from the target of interest and the background noise (signal-to-noise ratio; SNR). It is clear that a balance must be found between using short period gravity readings which significantly reduce the duration and cost of a survey, and still averaging for a long enough period to reduce the level of noise to an acceptable level whereby the SNR will be good enough to allow target detection. The SNR required to achieve predefined detection characteristics (detection probability and probability of false alarm) can be determined by the Neyman-Pearson decision rule (Poor, 2013). For example, to obtain a detection probability (P_d) of 0.9 and a probability of false alarm (P_{fa}) of 0.01, the required SNR should exceed 8 dB, which has been used as an acceptable level of confidence.

In order to calculate the SNR, since the current work is focused on the integration of environmental noise to gain accurate readings, only noise from microseism noise sources were considered (i.e. noise sources from variations in the instrument location between survey points such as signals from the terrain and density variations were ignored, as well as tidal and instrumental sources of noise) by using the standard deviation of the microseism noise. Wind noise was also assumed to be negligible, either due to the use of a windshield or due to calm conditions on a hypothetical site. In Figure 17 the dependence of the SNR for different targets and different durations of reading on the standard deviation of the microseism noise is presented. The readings with durations of 90 s and 300 s were analysed using 4 targets for a microgravity survey: 225 mm diameter sewer pipe, 24-inch (610 mm) natural gas pipe, 48-inch

(1210 mm) natural gas pipe, and a former military Royal Observer Corps (ROC) bunker (Royal Observer Corps Association (ROCA) Heritage Team, 2015). The larger two of these represent targets which may be detectable using the current instrument, whereas the smaller two are typical civil engineering targets, which are potentially detectable using future atom interferometer gravity sensors with a higher resolution and no drift with the capability of detecting smaller targets (Metje et al., 2011). The expected microgravity signals were obtained by approximating features as simple geometric shapes (e.g. cylinders, parallelepipeds) and using a bespoke forward model developed in Matlab®, based on formulae presented in the literature (Kearey, Brooks and Hill, 2013; Telford, Geldart and Sheriff, 1990). The expected gravity anomaly size was defined as the difference between the maximum and minimum values obtained from these simulations. These are presented in the first line of Table 1.

It can be clearly seen that the sewer pipe is invisible for current MEMS-based gravimeters even using comparatively long averaging intervals (300 s measurement cycles). The 24-inch natural gas pipes will be visible only in very quiet conditions. In contrast, the large natural gas pipeline and the military bunker can be detected if the level of the microseism noise is lower than 200 microGals for 90 s readings and during almost any levels of the microseism noise for 300 s readings. Thus the techniques presented would allow the survey manager to decide if a target of a given size might be detectable on a given day and determine an appropriate measurement cycle time per point.

Conclusions

It has been shown that the effects of microseism noise has a significant impact on the measurement of microgravity for geophysical surveying purposes, and can significantly affect the results if traditional survey methodologies are used, especially in terms of the measurement time per point. A new methodology has been developed which links the microseism noise manifesting itself on microgravity measurements with the freely available seismometer datasets, such as those collected by the British Seismmometer Network. This information can be used by practitioners for determining an optimal measurement strategy in terms of the measurement cycle time for a given day by generating a microseism noise map using data from preceding days. This allows a suitable timeframe to be allotted to complete the survey or, in extreme cases, it may be better to move the survey to a more suitable time, wasting less time and effort on unsuccessful surveys. This link had not been demonstrated before, but has significant impact on the survey industry and can reduce situations where targets of interest are not detected due to poorly understood microseism noise levels.

Acknowledgements

References

Ardhuin, F., Gualtieri, L. and Stutzmann, E. 2015. How ocean waves rock the Earth: Two mechanisms explain microseisms with periods 3 to 300 s. Geophysical Research Letters

Ardhuin, F. and Herbers, T.H.C. 2013. Noise generation in the solid Earth, oceans and atmosphere, from nonlinear interacting surface gravity waves in finite depth. Journal of Fluid Mechanics 716, 316–348

Ardhuin, F., Stutzmann, E., Schimmel, M. and Mangeney, A. 2011. Ocean wave sources of seismic noise. Journal of Geophysical Research - Oceans 116, C09004

Bidel, Y., Carraz, O., Charrière, R., Cadoret, M., Zahzam, N. and Bresson, A. 2013. Compact cold atom gravimeter for field applications. Applied Physics Letters 102

British Geological Survey. 2016. *BGS Broadband Seismic Station Book*. [cited 03/03/16]; Available from: http://www.earthquakes.bgs.ac.uk/monitoring/broadband_stationbook.html.

Essen, H.H., Krüger, F., Dahm, T. and Grevemeyer, I. 2003. On the generation of secondary microseisms observed in northern and central Europe. Journal of Geophysical Research: Solid Earth 108, 2506-2520

Field, E. and Jacob, K. 1993. The theoretical response of sedimentary layers to ambient seismic noise. Geophysical Research Letters 20, 2925-2928

GeoData Institute. 2015. *Channel Coastal Observatory Data Catalogue,*. [cited 26/02/16]; Available from: http://www.channelcoast.org/.

Gillot, P., Cheng, B., Imanaliev, A., Merlet, S. and Santos, F.P.D. 2016. The LNE-SYRTE cold atom gravimeter. In: The LNE-SYRTE cold atom gravimeter, pp. 1-3.

Goodkind, J.M. 1999. The superconducting gravimeter. Review of Scientific Instruments 70, 4131-4152

Hartmann, T. and Wenzel, H.-G. 1995. The HW95 tidal potential catalogue. Geophysical Research Letters 22, 3553-3556

Hassanpour, H., Mesbah, M. and Boashash, B. 2004. EEG spike detection using time-frequency signal analysis. Proceedings of the IEEE International Conference on Acoustics, Speech, and Signal Processing, 2004 (ICASSP '04). Vol. 5, Montreal, Canada, 421-424.

Hasselmann, K. 1963. A statistical analysis of the generation of microseisms. Rev. Geophys 1, 177-210

Hinton, A., Perea Ortiz, M., Lamb, A., Rammeloo, C., Stray, B., Voulazeris, G., Zhu, L., Kaushik, A., Lien, Y.-H., Niggebaum, A., Rodgers, A., Stabrawa, A., Boddice, D., Plant, S., Tuckwell, G.,

Bongs, K., Metje, N. and Holynski, M. 2017. A portable magneto-optical trap with prospects for atom interferometry in civil engineering. Philosophical Transactions of the Royal Society of London Series A

Jol, H. 2009. *Ground Penetrating Radar: Theory and Applications*. Elsevier Science, Amsterdam.

Kaufman, A.A., Alekseev, D. and Oristaglio, M. 2014. *Principles of Electromagnetic Methods in Surface Geophysics*. Elsevier Science, Amsterdam.

Kearey, P., Brooks, M. and Hill, I. 2013. *An Introduction to Geophysical Exploration*. Blackwell, Oxford.

Keller, G.V. and Frischknecht, F.C. 1966. *Electrical Methods in Geophysical Prospecting*. Pergamon Press Inc, Oxford.

Keys, R.G. 1981. Cubic Convolution Interpolation for Digital Image Processing. IEEE Trans. on Acoustics, Speech, and Signal Processing 29, 1153-1160

Longman, I.M. 1959. Formulas for Computing the Tidal Accelerations Due to the Moon and the Sun. Journal of Geophysical Research 64, 2351-2355

Merriam, J.B. 1992. Atmospheric pressure and gravity. Geophysical Journal International 109, 488-500

Met Office. 2016. *Storm Eva*. [cited 07/01/16]; Available from: http://www.metoffice.gov.uk/uk-storm-centre/storm-eva.

Metje, N., Chapman, D.N., Rogers, C.D.F. and Bongs, K. 2011. Seeing through the Ground: The Potential of Gravity Gradient as a Complementary Technology. Advances in Civil Engineering vol. 2011, Article ID 903758

Muquans. 2017. *https://www.muquans.com/index.php/products/aqg*. [cited 22/03/]; Available from: https://www.muquans.com/index.php/products/aqg.

Observatories and Research Facilities for European Seismology. 2013. *ORFEUS Data Center*. [cited 03/03/16]; Available from: http://www.orfeus-eu.org/.

Peters, A., Chung, K.Y. and Chu, S. 1999. Measurement of gravitational acceleration by dropping atoms. Nature 400, 849-852

Phillips, O.M. 1977. *The Dynamics of the Upper Ocean*. Cambridge University Press, Cambridge.

Poor, H.V. 2013. *An Introduction to Signal Detection and Estimation*. Springer New York.

Royal Observer Corps Association (ROCA) Heritage Team. 2015. *Preserved Monitoring Posts: England*. [cited 15/07/16]; Available from: http://www.roc-heritage.co.uk/england.html.

Scintrex Ltd. 2006. *Operating Manual for the CG5 Gravity Meter*. Scintrex Ltd., Concord, Ontario.

Seigel, H.O. 1995. *A Guide to High Precision Land Gravimeter Surveys*. Scintrex Ltd., Concord, Ontario.

Snadden, M.J., McGuirk, J.M., Bouyer, P., Haritos, K.G. and Kasevich, M.A. 1998. Measurement of the Earth's Gravity Gradient with an Atom Interferometer-Based Gravity Gradiometer. Physical Review Letters 81, 971-974

Sverdrup, H.U. and Munk, W.H. 1947. Wind, Sea, and Swell: Theory of Relations for Forecasting. Hydrographic Office 601, 44

Telford, W.M., Geldart, L.P. and Sheriff, R.E. 1990. *Applied Geophysics*. Cambridge University Press, Cambridge.

Traer, J., Gerstoft, P., Bromirski, P.D. and Shearer, P.M. 2012. Microseisms and hum from ocean surface gravity waves. Journal of Geophysical Research 117
UNESCO. 2016. *Stonehenge, Avebury and Associated Sites*. [cited 20/05/16]; Available from: http://whc.unesco.org/en/list/373.

Warburton, R.J. and Goodkind, J.M. 1977. The influence of barometric-pressure variations on gravity. Geophysical Journal of the Royal Astronomical Society 48, 281-292

Webb, S.C. 2008. The Earth's hum: The excitation of Earth normal modes by ocean waves. Geophys. J. Int 174, 542-566

Wilson, C.D.V. 1953. An analysis of the vibrations emitted by some man-made sources of microseisms. Proceedings of the Royal Society of London. Series A 217, 188-202

Yang, Y. and Ritzwoller, M.H. 2008. Characteristics of ambient seismic noise as a source for surface wave tomography. Geochemistry, Geophysics, Geosystems 9, Q02008

Captions

Figure 1: Noise spectra from long period measurements with two Scintrex CG5s

Figure 2: Typical variation of standard deviation of microseism noise observed in Birmingham on 11-27.02.2016 and a significant wave height, recorded in Cornwall at the station Wave Hub. A – 20/02/16 20:20 UTC, B – 26/02/16 01:05 UTC

Figure 3: Typical waveform of the microgravity signal

Figure 4: Spectra of the microgravity signals presented in Figure 3

Figure 5: Signal flow chain

Figure 6. Practical noise variance reduction as a function of observation time

Figure 7: Map of BGS broadband seismic stations. Black diamonds – processed stations, grey squares – other available stations.

Figure 8: Portable Windshield used to reduce the influence of wind on the measurements

Figure 9: Flow chart to determine the effective gain parameters

Figure 10: Typical result of cross-correlating a microgravity measurement with a seismic network data set

Figure 11. Scatter plot and linear regression of a 256 sec window of microgravity data with seismic data.

Figure 12: Noise prediction process

Figure 13: Typical ambient microgravity spectrum predicted and measured near CWF (Charnwood Forest, Leicestershire, UK)

Figure 14: Standard deviation of seismic noise versus standard deviation of microgravity noise.

Figure 15: a) Map of ambient microgravity noise on 20th August 2015 and b) Map of ambient microgravity noise on 25th December 2015. Point B corresponds to Birmingham; point D – Durrington.

Figure 16: The comparison between standard deviation of microseism noise and interpolated from ambient microgravity noise maps

Figure 17: Dependence of standard deviation of individual microgravity readings on power of microseism noise for 90 seconds (stars and a solid curve) and 5 minutes readings (dots and a dashed curve). Black solid strait lines show the maximum level of noise for the detection of sever pipe (1), natural gas pipe (2), big natural gas pipeline (3) and a military bunker (4).

Table 1: Expected gravity anomaly and required level of noise for successful target detection
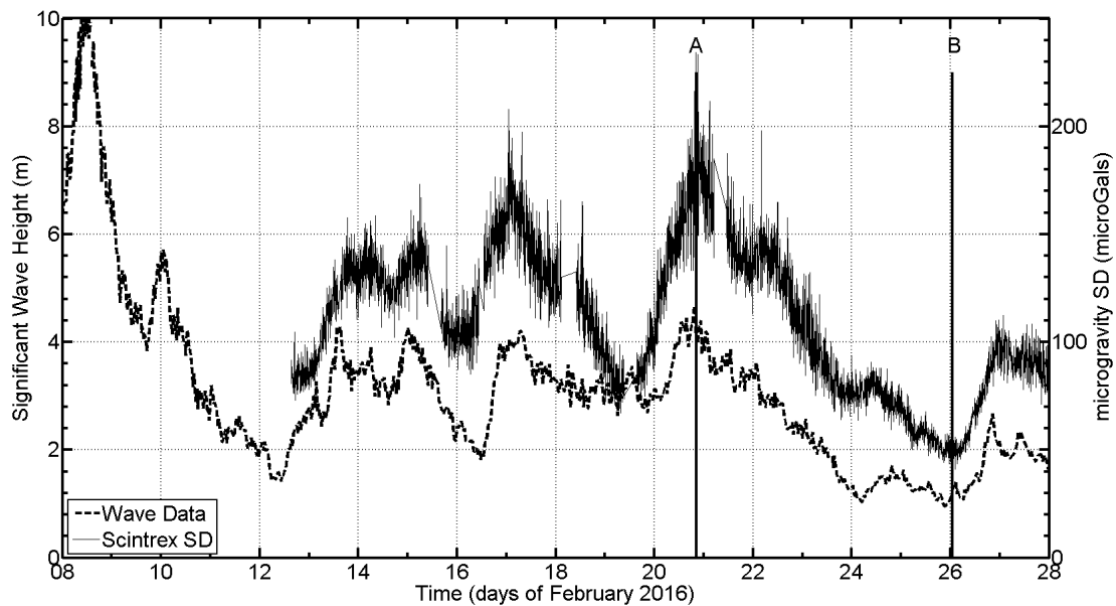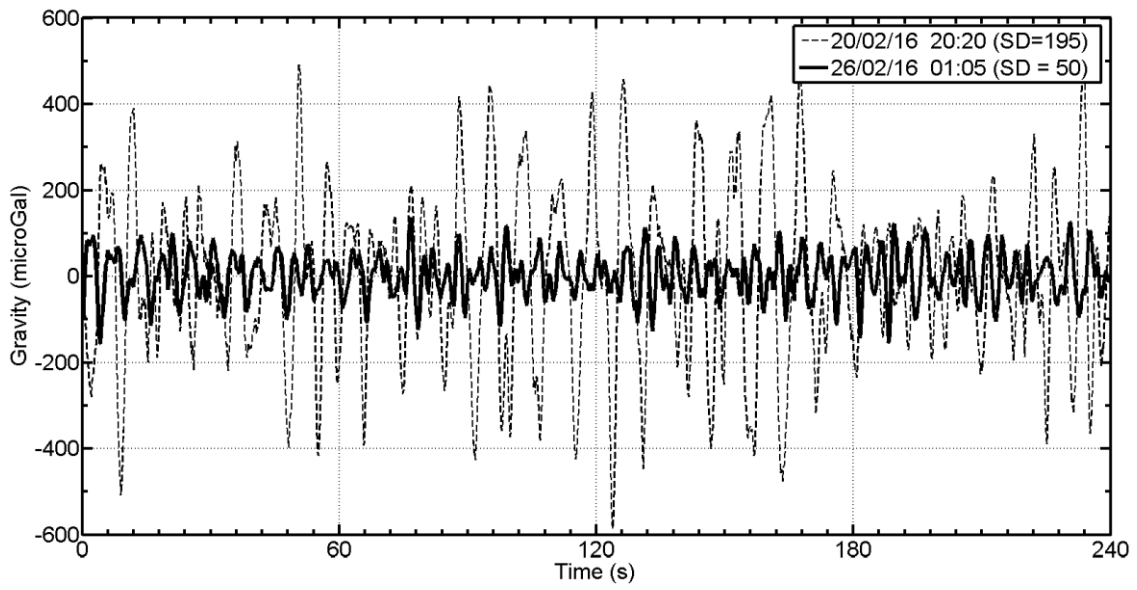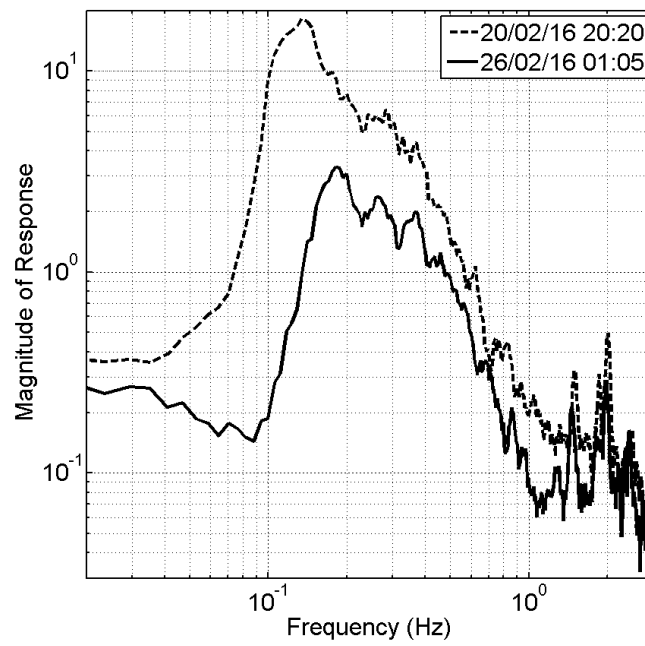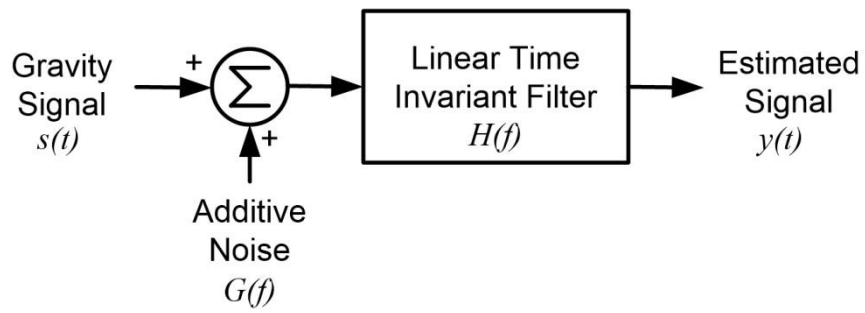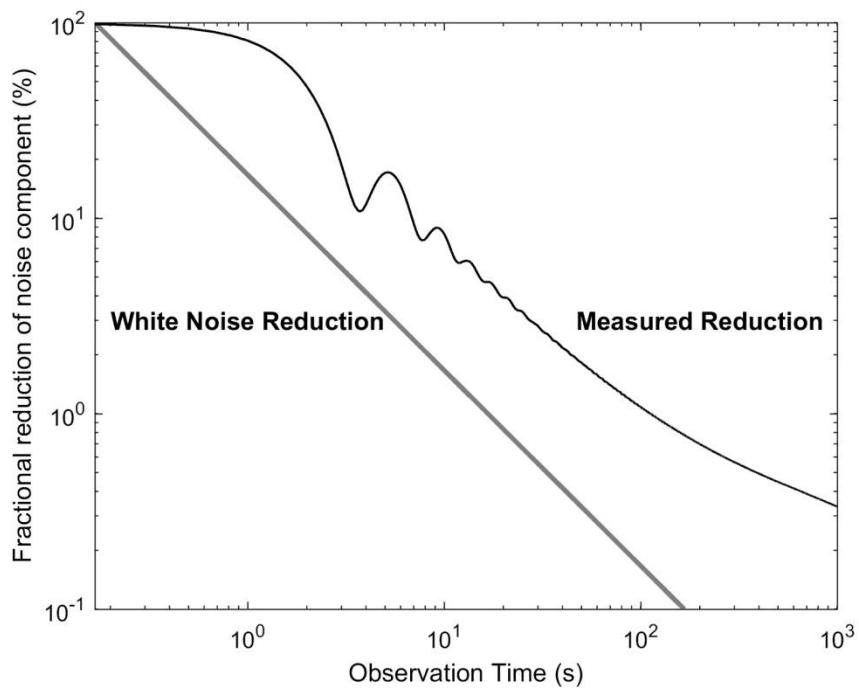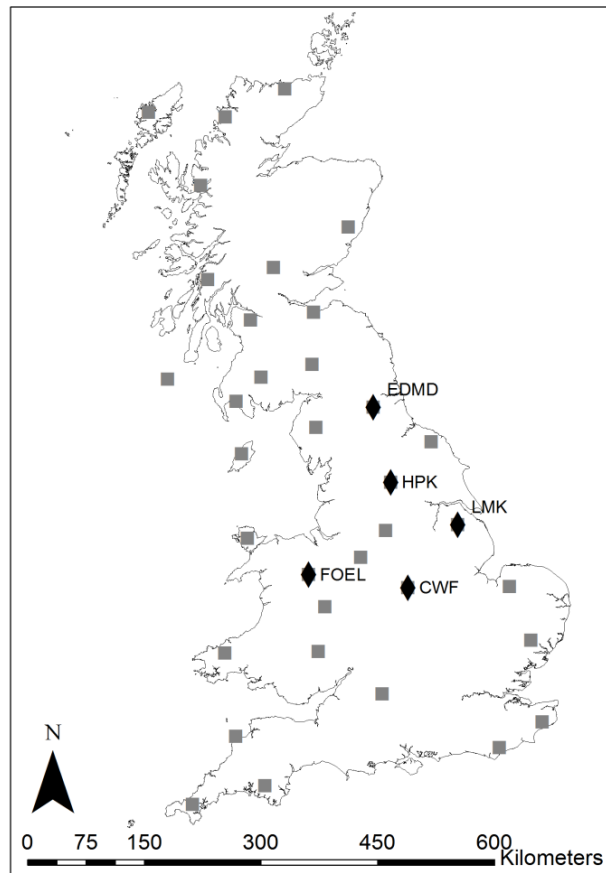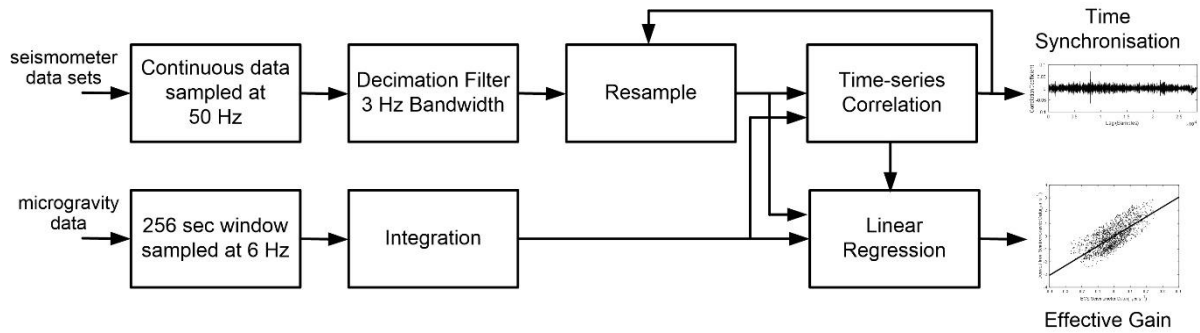
Tables

Table 1: Expected gravity anomaly and required level of noise for successful target detection

Name of target (d – diameter, h – depth to the geometrical centre)	Sewer Pipe (d=0.225 m, h=1.2 m)	Gas Pipe (d=0.61 m, h=3 m)	Gas Pipe (d=1.2 m, h=1.8 m)	Military bunker (V = 30 m^3, h=3 m)
Expected gravity anomaly (microGals)	1	2.5	15.9	29.0
Maximum SD of noise (microGals)	0.16	0.38	2.41	4.39

Figures

Figure 1: Noise spectra from long period measurements with two Scintrex CG5s

Figure 2: Typical variation of standard deviation of microseism noise observed in Birmingham on 11-27.02.2016 and a significant wave height, recorded in Cornwall at the station Wave Hub. A – 20/02/16 20:20 UTC, B – 26/02/16 01:05 UTC

Figure 3: Typical waveform of the microgravity signal

Figure 4: Spectra of the microgravity signals presented in Figure 3

Figure 5: Signal flow chain

Figure 6: Practical noise variance reduction as a function of observation time

Figure 7: Map of BGS broadband seismic stations (Black diamonds – processed stations; grey squares – other available stations)

Figure 8: Portable Windshield used to reduce the influence of wind on the measurements

Figure 9: Flow chart to determine the effective gain parameters

Figure 10: Typical result of cross-correlating a microgravity measurement with a seismic network data set

Figure 11: Scatter plot and linear regression of a 256 sec window of microgravity data with seismic data.
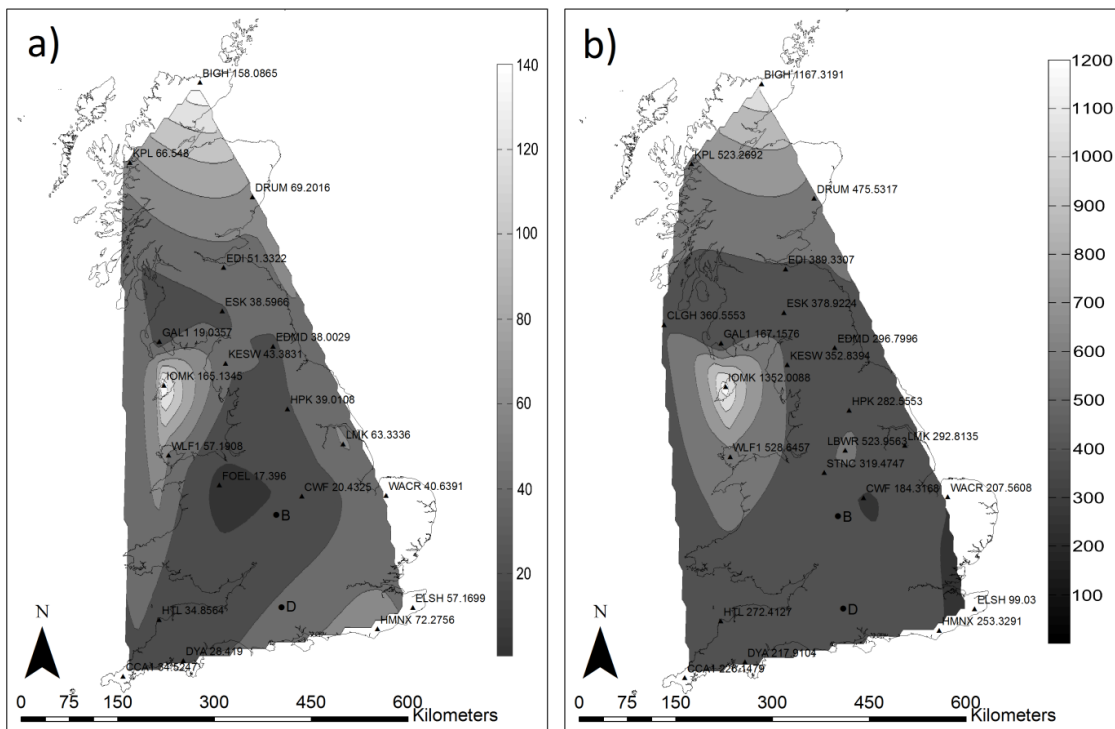
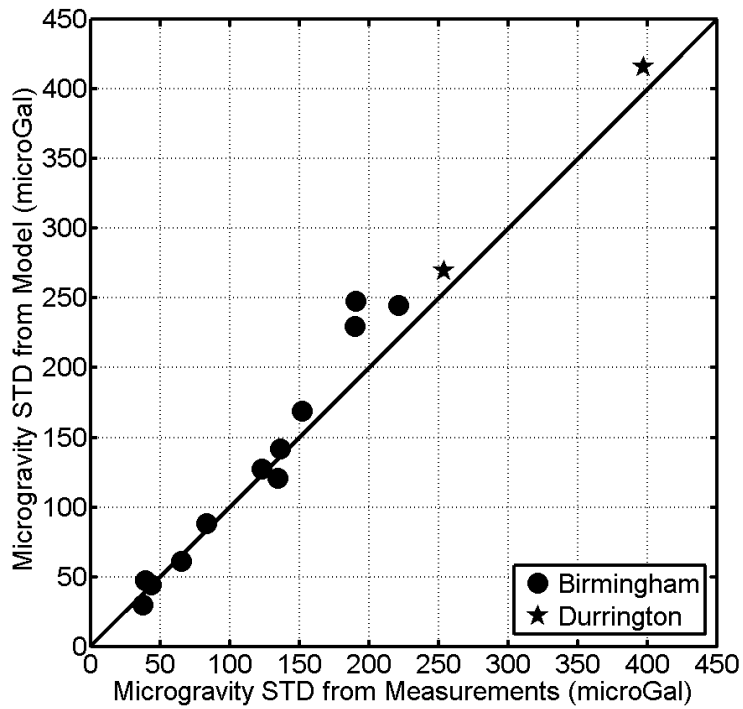**Figure 12: Noise prediction process**

Figure 13: Typical ambient microgravity spectrum predicted and measured near CWF (Charnwood Forest, Leicestershire, UK)
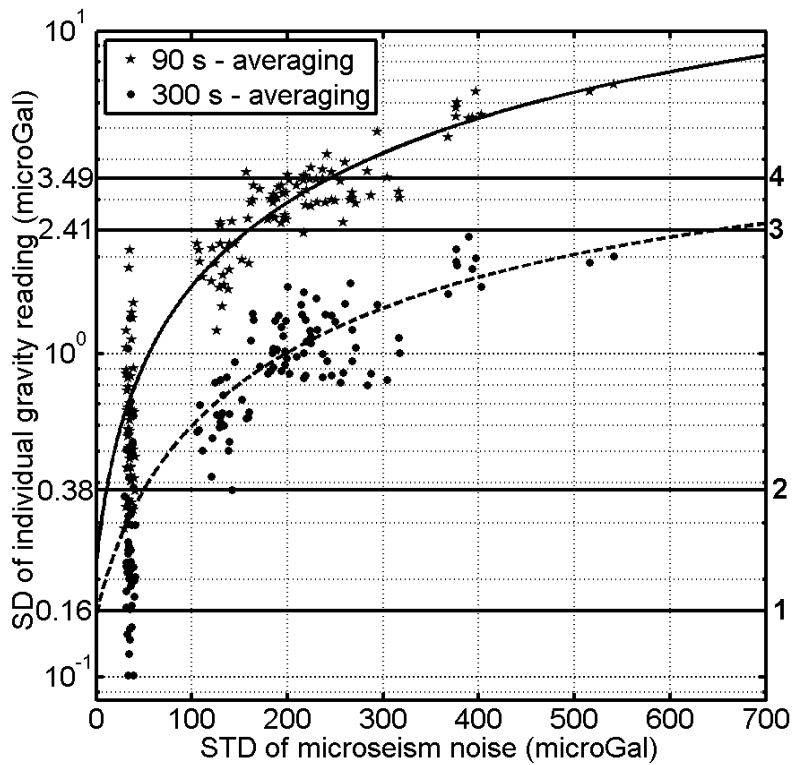
Figure 14: Standard deviation of seismic noise versus standard deviation of microgravity noise

Figure 15: a) Map of ambient microgravity noise on 20th August 2015 and b) Map of ambient microgravity noise on 25th December 2015 (Point B corresponds to Birmingham; point D – Durrington)

Figure 16: The comparison between standard deviation of microseism noise and interpolated from ambient microgravity noise maps

Figure 17: Dependence of standard deviation of individual microgravity readings on power of microseism noise for 90 seconds (stars and a solid curve) and 5

minutes readings (dots and a dashed curve). Black solid straight lines show the maximum level of noise for the detection of sewer pipe (1), natural gas pipe (2), big natural gas pipeline (3) and a military bunker (4)